The Construction and Analysis of ceRNA Network and Immune Infiltration in Kidney Renal Clear Cell Carcinoma

Lugang Deng [1], Zhi Qu [2], Peixi Wang [2], Nan Liu [1, 2, 3, *]

[1] School of Public Health, Guangzhou Medical University, Guangzhou, 511436, P. R. China

[2] Institute of Chronic Disease Risks Assessment, School of Nursing and Health, Henan University, Kaifeng, 475004, P. R. China

[3] Pinghu Hospital, Health Science Center, Shenzhen University, Shenzhen, 518116, P. R. China.

*Corresponding author:

Nan Liu

13688869875@163.com

ORCID: orcid.org/0000-0002-8895-3169

Abstract

Background: Kidney renal clear cell carcinoma (KIRC) has the highest invasion, mortality and metastasis of the renal cell carcinomas and seriously affects patients' quality of life. However, the composition of the immune microenvironment and regulatory mechanisms at transcriptomic level such as ceRNA of KIRC are still unclear.

Methods: We constructed a ceRNA network associated with KIRC by analyzing the long noncoding RNA (lncRNA), miRNA and mRNA expression data of 506 tumor tissue samples and 71 normal adjacent tissue samples downloaded from the Cancer Genome Atlas (TCGA) database. In addition, we estimated the proportion of 22 immune cell types in these samples through "The Cell Type Identification by Estimating Relative Subsets of RNA Transcripts". Based on the ceRNA network and immune cells screened by univariate Cox analysis and Lasso regression, two nomograms were constructed to predict the prognosis of patients with KIRC. Receiver operating characteristic curves (ROC) and calibration curves were employed to assess the discrimination and accuracy of the nomograms. Consequently, co-expression analysis was carried out to explore the relationship between each prognostic gene in a Cox proportional hazards regression model of ceRNA and each survival-related immune cell in a Cox proportional hazards regression model of immune cell types to reveal the potential regulatory mechanism.

Results: We established a ceRNA network consisting of 12 lncRNAs, 25 miRNAs and 136 mRNAs. Two nomograms containing seven prognostic genes and two immune cells, respectively, were successfully constructed. Both ROC [Area Under Curves (AUCs) of 1, 3 and 5-year survival in the nomogram based on ceRNA network: 0.779, 0.747 and 0.772; AUCs of 1, 3 and 5-year survivals in nomogram

based on immune cells: 0.603, 0.642 and 0.607] and calibration curves indicated good accuracy and clinical application value of both models. Through co-correlation analysis between ceRNA and immune cells, we found both LINC00894 and KIAA1324 were positively correlated with follicular helper T (Tfh) cells and negatively correlated with resting mast cells.

Conclusions: Based on the ceRNA network and tumor-infiltrating immune cells, we constructed two nomograms to predict the survival of KIRC patients and demonstrated their value in improving the personalized management of KIRC.

Keywords: Kidney renal clear cell carcinoma; TCGA; Competing endogenous RNA network; Immune cell; Prognosis

Introduction

Renal cell carcinoma is a malignant kidney tumor that the American Cancer Society reports was diagnosed in 65,340 patients, and caused 14,970 deaths, in the United States during 2018 (1). It is a serious health problem worldwide, and the economic burden of the disease has steadily increased during the last century (2). Kidney renal clear cell carcinoma (KIRC) is the subtype of renal cell carcinoma with the highest invasiveness, mortality and metastasis rates (3); it is typically screened and diagnosed through computed tomography (CT), magnetic resonance imaging (MRI) and pathological section testing in the clinic (4). Several difficulties continue to make KIRC a challenge to treat, including its stealth in early stages, a lack of effective biomarkers, radiation risks and the high cost of diagnostic imaging required. Underlying biomarkers and molecular mechanisms for the prevention, diagnosis and prognosis of KIRC require further studies.

Long noncoding RNAs (lncRNAs) contain more than 200 nucleotides without the function of encoding proteins and have achieved attention recently because of their potential for exploring novel biomarkers in diseases and for elucidating mechanisms of biological processes (5, 6). Current research reveals that lncRNA plays an important role in the genesis and development of tumors through interactions with competing endogenous RNA (ceRNA) or by acting as microRNA sponges (7). Tumor-infiltrating immune cells are a major component of the tumor microenvironment and affect the clinical outcomes and pathological staging of multiple tumor types (8, 9). Some studies suggest lncRNA can affect tumor development and tumor immune cell microenvironment through the ceRNA network (10-12). Therefore, exploring interactions between the ceRNA network and various immune cells in the development of KIRC is essential.

In this study, we construct a ceRNA network related to the occurrence and development of KIRC using transcriptome and clinical data from the Cancer Genome Atlas (TCGA) to explore potential molecular mechanisms. In addition, we used "The Cell Type Identification by Estimating Relative Subsets of RNA Transcripts algorithm" (CIBERSORT) algorithm to assess differences in the composition of immune cells within tumor tissues and normal tissues. Furthermore, predictive nomograms were constructed based on the ceRNA network and on significant immune cells. Finally, we evaluated the relationship between tumor-infiltrating immune cells and the ceRNA network to identify the underlying regulatory mechanisms.

Materials and methods

Data source and selection

A flowchart illustrating the research process of our study is provided in Figure 1. Data on lncRNA, miRNA and mRNA expression of KIRC patients were downloaded from the Cancer Genome Atlas (TCGA) database (https://portal.gdc.cancer.gov/) through the GDC data transfer tool. Relevant clinical information including age, gender, survival data (vital status, days to death and days to last follow-up), grade and TNM stage of tumor tissues was also obtained for further analysis. We excluded samples with incomplete survival or pathological staging data, as well as duplicate samples. Only samples with both mRNA and miRNA expression profiles were included in this study. Correspondingly, the adjacent and paired normal tissues collected from the included patients was setted as the control group.

Figure 1

Differential expression analysis

Based on the HTSeq-Counts data of included samples, we used the "DESeq2"

package (13) (http://bioconductor.org/packages/DESeq2/) of Bioconductor to screen for differentially expressed lncRNAs (DElncRNAs), miRNAs (DEmiRNAs) and mRNAs (DEmRNAs) between KIRC tissue and normal adjacent tissue. The log fold change (FC) criterion for differential expression was set as $|\log_2(FC)| > 1$ and the false discovery rate (FDR) at < 0.05. For the differential expression results of each type of RNA, volcano plots and heatmaps were generated through R packages "ggpolt2" and "pheatmap."

Construction of lncRNA-miRNA-mRNA ceRNA network and survival analysis

Using the differential expression results, we predicted the miRNAs-lncRNAs interactions and the miRNAs-mRNAs interactions based on the starBase v2.0 database (14, 15) (http://starbase.sysu.edu.cn/starbase2/index.php), which contained the miRNA-target interactions overlapped with CLIP-Seq data. We conducted hypergeometric tests and correlation analysis to filter the predicted interactions with FDR < 0.05 as the screening criteria. In addition, the lncRNA-miRNA-mRNA regulatory network of KIRC was visualized using Cytoscape v.3.8.1 (http://cytoscape.org/) (16). Besides, we conducted a Kaplan-Meier (K-M) survival curve analysis to assess the prognostic value of genes in the KIRC ceRNA network.

ceRNA network: Cox proportional hazards regression model

Firstly, significant variables were screened for integration into the initial Cox model using univariate Cox analysis. Next, a least absolute shrinkage and selection operator (Lasso) regression was employed to further evaluate the fitness of multifaceted models and filter variables. Finally, we generated a nomogram of from multivariate Cox proportional hazards regression models to predict the prognosis of KIRC patients. To confirm the discrimination and precision of the nomogram, receiver operating characteristic curves (ROC) and calibration curves were employed. In addition, we

calculated the risk score of each patient and then divided patients into high and low risk groups based on the median to conduct a K-M survival curve analysis.

Tumor-infiltrating immune cells: CIBERSORT estimation and survival analysis

To analyze differences between the two groups at the level of immune cells, and explore the connection between key biomarkers in the ceRNA network and immune cells, we estimated the proportion of 22 kinds of immune cell types in 506 tumor tissues and 71 normal adjacent tissues by CIBERSORT (17) (http://cibersort.stanford.edu/), an algorithm for characterizing cell composition of complex tissues from their gene expression profiles. Only samples with CIBERSORT output of $P < 0.05$ were included in further analysis. After screening samples, we searched for immune cells with significant differences between cancer tissues and normal adjacent tissues, as indicated by a Wilcoxon rank-sum test. A K-M survival curve analysis was performed to evaluate the relationship between the content of different immune cells and the overall survival of KIRC patients.

Tumor-infiltrating immune cells: Cox proportional hazards regression model

Immune cells with significant effects in univariate Cox analysis were integrated into the initial Cox model and the Lasso regression again used to evaluate the fitness of multifaceted models and filter variables further. As above, we constructed a nomogram based on the multivariate model of immune cells, and used ROC and calibration curves to confirm the discrimination and precision of the nomogram. Similarly, we conducted a K-M survival curve analysis by dividing patients into high and low risk groups according to the median of risk score. Finally, a Pearson correlation analysis was used to explore the relationship between genes and immune cells.

Statistical Analysis

Only two-sided *P*-values < 0.05 was considered statistically significant. All statistical analyses were conducted in R version 4.0.2 software (Institute for Statistics and Mathematics, Vienna, Austria; www.r-project.org) (packages: corrplot, DESeq2, GDCRNATools, ggplot2, glmnet, pheatmap, rms, survival, survminer, timeROC).

Results

Differential expression in lncRNAs , miRNAs and mRNAs

After screening the samples of TCGA-KIRC, we constructed an experimental group and a control group containing of 506 tumor tissues and 71 normal adjacent tissues, respectively. Compared to the control group, we identified 357 DElncRNAs (287 up-regulated and 70 down-regulated), 132 DEmiRNAs (61 up-regulated and 71 down-regulated) and 3092 DEmRNAs (2032 up-regulated and 1060 down-regulated) using the cutoffs of the $|\log_2(FC)| > 1$ and FDR < 0.05 (Figure 2a-g).

Figure 2

Figure 3

Table 1

Construction of lncRNA-miRNA-mRNA ceRNA network and survival analysis

Using the starBase v2.0 database and ceRNA theory, a lncRNA-miRNA-mRNA ceRNA network consisting of 173 genes (12 lncRNAs, 25 miRNAs and 136 mRNAs) was established (Figure 3a and Table 1). A K-M survival curve analysis to assess the prognostic value of nodes in the ceRNA network revealed 83 genes (10 lncRNAs, 7 miRNAs and 66 mRNAs) related to the overall survival of KIRC patients. Survival curves of the top three (according to *P*-value) lncRNAs (PVT1, AC005154.1, AC015813.1), miRNAs (hsa-miR-21-5p, hsa-miR-130b-3p, hsa-miR-204-5p), and mRNAs (MXD3, VPS13D, KCNN4) are shown in Figures 3b-d, e-g and h-j,

185 respectively.

186 ***ceRNA network: Cox proportional hazards regression model***

187 Univariate Cox analysis applied to filter genes in the ceRNA network retained 97
188 genes for incorporation into the initial model (Table S1). Lasso regression analysis
189 indicated that 15 genes were statistically significant in this model. Subsequently, a
190 Cox proportional hazards regression model with seven genes was established through
191 further screening of key genes based on the Akaike Information Criterion (AIC).
192 Finally, we constructed a nomogram to predict the 1, 3 and 5-year overall survival
193 probability of KIRC patients. ROC [Area Under Curves (AUCs)] for the model gave
194 1, 3 and 5-year survivals of 0.779, 0.747 and 0.772, respectively, which reflected the
195 discrimination and precision of the nomogram with calibration curves (Figure 4).
196 Overall survival (based on K-M curves) of the high-risk group is lower than that of
197 the low-risk group (Figure S1). Survival curves of the genes in the model are also
198 provided in Figure S1.

199 **Figure 4**

200 ***Tumor-infiltrating immune cells: CIBERSORT estimation and survival analysis***

201 The analysis by CIBERSORT identified five normal tissue samples and 206 tumor
202 tissue samples for inclusion in subsequent analysis ($P < 0.05$) and the proportions of
203 22 immune cells in each sample are displayed in the histogram and heat map of
204 Figure 5. A Wilcoxon rank-sum test showed that naive B cells ($P < 0.001$), plasma
205 cells ($P < 0.001$), CD8 T cells ($P = 0.014$), CD4 naive T cells ($P < 0.001$), CD4
206 memory resting T cells ($P = 0.013$), regulatory (Tregs) T cells ($P = 0.015$), gamma
207 delta T cells ($P = 0.021$), resting dendritic cells ($P = 0.016$) and resting mast cells ($P =$
208 0.048) all varied between the two tissue sample types (Figure 5c). Based on the results
209 of K-M survival curve analysis, five immune cells, including memory B cells, plasma

cells, follicular helper T (Tfh) cells, T regulatory (Tregs) cells and resting mast cells were related to overall survival of KIRC patients (Figure S2).The clinical correlation of 22 immune cells is displayed in Figure S3.

Figure 5

Tumor-infiltrating immune cells: Cox proportional hazards regression model

After filtering based on univariate Cox analyses (Table S2), two of 22 immune cells (Tfh and resting mast cells) were incorporated into the initial regression model. Lasso regression analysis and AIC were then employed for further optimization of the model, and both cells were kept in the final Cox proportional hazards regression model. A nomogram was developed to predict the 1, 3 and 5-year overall survival probability of KIRC patients based on the model. Both the ROC (AUCs of 1, 3 and 5-year survivals: 0.603, 0.642 and 0.607) and the calibration curves suggested that the nomogram had good accuracy (Figure 6). The K-M survival curves suggested that significant differences existed in the overall survival of the high versus low-risk group (Figure S4).

Figure 6

Co-expression analysis of key genes and immune cells

Pearson correlation analysis was used to explore the co-expression pattern between 22 types of immune cells (Figure 7a). Similarly, the co-expression relationship between the key biomarkers and immune cells of the two models is illustrated in Figure 7b. Tfh cells are positively correlated with LINC00894 (Figure 7c, R = 0.36, $P < 0.001$) and KIAA1324 (Figure 7d, R = 0.39, $P < 0.001$), while resting mast cells are negatively correlated with LINC00894 (Figure 7e, R = -0.32, $P < 0.001$) and KIAA1324 (Figure 7f, R = -0.30, $P < 0.001$).

Figure 7

Validation of the correlation between key genes and immune cells

Multiple databases were searched to verify the correlation between the key genes (LINC00894 and KIAA1324) and immune cells (Tfh cells and resting mast cells) identified. B cell lymphoma 6 (BCL6), CXCL13, CD10 (MME), ICOS and PD-1 (PDCD1) were the most common surface markers of Tfh cells in the CellMarker database (Figure S5). In the Oncomine™ platform, we explored the expression of KIAA1324 and Tfh markers among various cancers. KIAA1324, BCL6, CXCL13, ICOS and PDCD1 were highly expressed and MME was downregulated in KIRC compared to normal kidney tissue (Figure S6); median rank and *P*-values are listed in Table S3.

Using the Gene Expression Profiling Interactive Analysis (GEPIA), KIAA1324 is positively correlated with CXCL13, ICOS and PDCD1 in KIRC (Figure S7), and LINC00894 is positively correlated with BCL6, ICOS and PDCD1 in KIRC (Figure S8). Similarly, the results of the LinkedOmics database showed that KIAA1324 was positively correlated with BCL6, CXCL13, ICOS and PDCD1 in KIRC. In addition, the expression of KIAA1324 was significantly different among tumor stages and related to tumor purity in KIRC (Figure S9).

Discussion

KIRC is one of the most common and malignant subtypes of kidney tumors (3). However, because of limitations in early detection and a lack of sensitive biomarkers, patients with KIRC typically have a poor prognosis. Recently, ceRNA was identified as playing a potentially important role in the molecular regulatory function of tumorigenesis and growth, and in affecting differences in immune-infiltrating cells within multiple tumors. In this study, we investigated the role and connection of the

ceRNA network and immune infiltration in KIRC to explore key prognostic biomarkers and potential regulatory mechanisms.

We established a ceRNA network consisting of 12 lncRNAs, 25 miRNAs and 136 mRNAs and compared the composition differences of immune cells related to KIRC. Based on the results, two prediction nomograms consisting of seven genes and two immune cells, respectively, were constructed to evaluate overall survival. A correlation analysis of the key factors in both nomograms indicated that both LINC00894 (lncRNA) and KIAA1324 (protein-coding RNA) were positively correlated with Tfh cells and negatively correlated with resting mast cells. Consequently, we infer that ceRNA regulatory function, in which both LINC00894 and KIAA1324 participate, and Tfh cells and resting mast cells may play a crucial role in the development and treatment of KIRC.

LINC00894 is lncRNA derived from a locus on the X chromosome that is differentially expressed in various cancers (18). Similar to our work, Liang (19) reported that LINC00894 was a tumor-special lncRNA in KIRC that was upregulated in tumor tissues and correlated with overall survival time. Epithelial-to-mesenchymal transition (EMT) regulating miRNAs regulate drug resistance and cancer progression and metastasis (20, 21). LINC00894 can inhibit the TGF-β2/ZEB1 signaling pathway by acting as the sponge of EMT-regulating miR-200, or can be upregulated by ERα activation and positively regulate the expression of miR-200a-3p and miR-200b-3p, which results in induction of the TGF-β2/ZEB1 signaling pathway to reduce the occurrence of drug resistance in breast cancers (18, 22, 23). In our study, LINC00894 might suppress the expression of hsa-miR-342-3p, which has an important role in progression, staging and metastasis of various cancers (24-27). In view of the upregulation of hsa-miR-342-3p contributing to gefitinib resistance via targeting

CPA4 in non-small cell lung cancer (28), we speculate that LINC00894 is involved in the progression of cancer and may be a promising treatment target to eliminate drug resistance in patients with KIRC.

KIAA1324, also known as EIG121, encodes a 1013 amino acid transmembrane protein that shows high sequence conservation among different species. In type I endometrial cancer (estrogen-related), the expression of KIAA1324 is upregulated, but it is downregulated in type II endometrial cancer (not estrogen-related), which is more malignant than type I (29). KIAA1324 may be a novel suppressor, being epigenetically downregulated in gastric cancer (30); in addition, its high expression in endometrial and pancreatic carcinoma predicts improved survival (31, 32). However, increased expression of KIAA1324 in ovarian cancer is associated with a poor prognosis (33). These studies indicate that KIAA1324 may exhibit different biological functions in various cancers. Furthermore, recent mechanistic studies reveal that KIAA1324 is localized to endosome-lysosome compartments and associated with autophagy, which helps protect cells from cell death by upregulating the autophagy pathway under unfavorable conditions, such as starvation or chemotherapy (34). Therefore, we infer that overexpressed KIAA1324 helps cancer cells proliferate and resist chemotherapy in KIRC.

In this study, we explored five among 22 types of immune cells related to patient prognosis, and screened out the Tfh cells and resting mast cells to construct a Cox proportional hazards regression model, which evaluation of its AUC suggests has clear clinical value. Gou et al. (35) also explored the relationship between immune cells and renal cell carcinoma, and similar to our research, found Tfh cells were associated with poor prognosis and resting mast cells were positively associated with long term survival.

Under the action of myeloid professional antigen presenting cells (APC), naive CD4+ T cells could differentiate into Tfh cells and non-Tfh effector cells (such as Th1, Th2, or Th17 cells) (36). Therefore, Tfh cells are a specialized subset of CD4+ T cells that help B cells respond to antigens (37), which is, in turn, depends on the expression of transcriptional factor B cell lymphoma 6 (BCL6) (38). In the past decade, several studies have revealed a potential connection between Tfh cells and infiltrated tumors. Amé-Thomas et al. (39) demonstrated that Tfh cells protect follicular lymphoma malignant B cells from spontaneous and rituximab-induced apoptosis by upregulating CD40L and IL-4, which might lead to a worse prognosis. In non-small cell lung cancer (NSCLC) tumor tissues, the proportion of Tfh cells is increased, suggesting that Tfh cells might play an important role in estimating the poor survival of NSCLC patients (40). In addition, Tfh cell abundance is known to improve prognosis of patients with breast cancer or colorectal cancer (41, 42), which indicates the value of Tfh cells against tumors through immune responses.

Mast cells, both resting and activated, are large granulated innate immune cells found predominantly in sites between the host and its external environment, such as skin, respiratory mucosa, and the gastrointestinal tract (43). The activation of mast cells is related to various stimuli received by numerous receptors on the cell surface, such as pathogens, neuropeptides, cytokines, growth factors, toxins, basic compounds, complement, immune complexes, etc. (44). Recent studies have shown that the association between mast cells and cancer is two-sided, including both involvement in, and protection against, tumor progression. Xu et al. (45) constructed a prognosis-associated microRNA–mast cell network in lung adenocarcinoma, and found resting mast cell numbers were closely related to better overall survival and disease-free survival (DFS), while activated mast cells were related to poor survival.

335 miR-30a and miR-550a are also involved in the regulation of immune response by
336 acting as the promoter and suppressor of resting mast cells, respectively. In contrast,
337 mast cells in hepatocellular carcinoma are mostly resting, inactivation of mast cells
338 can promote immune escape, which is beneficial to tumor growth (46).

339 Our research inevitably has some limitations that should be recognized. First, our
340 research data was obtained from public databases. The limited data means that the
341 clinical pathological parameters are incomplete, which can lead to potential errors and
342 biases. Secondly, we have not taken the heterogeneity of the immune
343 microenvironment associated with the location of immune infiltration into
344 consideration. In other words, the accuracy and applicability of the prediction models
345 will be affected by the heterogeneity of tissue subtypes. In addition, the data series
346 used in this study are all from Western countries, so applying the research conclusions
347 to Asian countries has certain bias and may be inappropriate. As well, the lack of cell
348 markers for resting mast cells leads to incomplete validation in our study. Lastly, this
349 study is not a biological mechanism research, as it lacks experiments on the
350 interaction mechanisms between ceRNA and immune cells. Despite limitations of the
351 study, we did combine tumor infiltrating immune cells with a ceRNA network for
352 analysis in KIRC, which not only constructed two normograms with clinical
353 predictive value, but also identified a correlation between two key prognostic
354 molecules and two prognosis-related immune cells, providing novel directions for
355 future research.

356

357 ## Conclusions

358 Based on tumor-infiltrating immune cells and ceRNA networks, we constructed two
359 nomograms to predict survival of KIRC patients. The high AUC values we obtained

reflect the utility of this approach, which provides clinicians with more comprehensive clinical information through the models to improve individual management of KIRC patients. In addition, our study suggests that LINC00894, KIAA1324, Tfh cells and resting mast cells are significantly related to the prognosis of KIRC patients and we infer that LINC00894 and KIAA1324 might interact with Tfh cells and resting mast cells to affect the progression of KIRC. This study also provides new ideas for the pathogenesis and clinical treatment of KIRC.

Author contribution

ZQ and NL conceived the idea and designed the study. LD conducted the data analysis and visualization. PW performed the data interpretation and literature collection. LD and NL wrote the manuscript. ZQ and NL contributed to the revision of the manuscript draft. All authors read and approved the final manuscript.

Data availability statement

The dataset (TCGA-KIRC) analyzed in this study is publicly available in TCGA (https://tcga-data.nci.nih.gov/tcga/).

Declaration of competing interest

We declare that no potential competing interests exist.

Acknowledgement

This work was supported by National Natural Science Foundation of China (No. 81872584) and (No. 81472941), National 863 Young Scientist Program (No. 2015AA020940), Key Scientific Research Project Plan of Henan Province (No. 21A330001), Natural Science Foundation of Guangdong Province (No. 2016A030313138), Key Projects of Guangzhou Science and Technology Program (No. 201704020056), Interdisciplinary Research for First-class Discipline Construction Project of Henan University (No. 2019YLXKJC04) and Scientific Research Project for University of Education Bureau of Guangzhou (No. 201831841).

References

1. R. L. Siegel, K. D. Miller and A. Jemal: Cancer statistics, 2018. *CA: A Cancer Journal for Clinicians*, 68(1), 7-30 (2018) doi:10.3322/caac.21442
2. J. J. Hsieh, M. P. Purdue, S. Signoretti, C. Swanton, L. Albiges, M. Schmidinger, D. Y. Heng, J. Larkin and V. Ficarra: Renal cell carcinoma. *Nature Reviews Disease Primers*, 3(1), 17009 (2017) doi:10.1038/nrdp.2017.9
3. W. Xiao, X. Wang, T. Wang and J. Xing: Overexpression of BMP1 reflects poor prognosis in clear cell renal cell carcinoma. *Cancer gene therapy*, 27(5), 330-340 (2020) doi:10.1038/s41417-019-0107-9
4. J. J. Morrissey, V. M. Mellnick, J. Luo, M. J. Siegel, R. S. Figenshau, S. Bhayani and E. D. Kharasch: Evaluation of Urine Aquaporin-1 and Perilipin-2 Concentrations as Biomarkers to Screen for Renal Cell Carcinoma: A Prospective Cohort Study. *JAMA Oncology*, 1(2), 204-212 (2015) doi:10.1001/jamaoncol.2015.0213
5. T. Nagano and P. Fraser: No-Nonsense Functions for Long Noncoding RNAs. *Cell*, 145(2), 178-181 (2011) doi:https://doi.org/10.1016/j.cell.2011.03.014
6. J. J. Quinn and H. Y. Chang: Unique features of long non-coding RNA biogenesis and function. *Nature Reviews Genetics*, 17(1), 47-62 (2016) doi:10.1038/nrg.2015.10
7. Y. Tay, J. Rinn and P. P. Pandolfi: The multilayered complexity of ceRNA crosstalk and competition. *Nature*, 505(7483), 344-352 (2014) doi:10.1038/nature12986

411 8. W. Hong, Y. Gu, R. Guan, D. Xie, H. Zhou and M. Yu: Pan-cancer analysis of the
412 CASP gene family in relation to survival, tumor-infiltrating immune cells and
413 therapeutic targets. *Genomics*, 112(6), 4304-4315 (2020)
414 doi:https://doi.org/10.1016/j.ygeno.2020.07.026
415 9. Y. Gao, S. Chen, S. Vafaei and X. Zhong: Tumor-Infiltrating Immune Cell
416 Signature Predicts the Prognosis and Chemosensitivity of Patients With Pancreatic
417 Ductal Adenocarcinoma. *Frontiers in oncology*, 10, 557638-557638 (2020)
418 doi:10.3389/fonc.2020.557638
419 10. M. Xu, X. Xu, B. Pan, X. Chen, K. Lin, K. Zeng, X. Liu, T. Xu, L. Sun, J. Qin, B.
420 He, Y. Pan, H. Sun and S. Wang: LncRNA SATB2-AS1 inhibits tumor metastasis and
421 affects the tumor immune cell microenvironment in colorectal cancer by regulating
422 SATB2. *Molecular Cancer*, 18(1), 135 (2019) doi:10.1186/s12943-019-1063-6
423 11. D. Huang, J. Chen, L. Yang, Q. Ouyang, J. Li, L. Lao, J. Zhao, J. Liu, Y. Lu, Y.
424 Xing, F. Chen, F. Su, H. Yao, Q. Liu, S. Su and E. Song: NKILA lncRNA promotes
425 tumor immune evasion by sensitizing T cells to activation-induced cell death. *Nature*
426 *Immunology*, 19(10), 1112-1125 (2018) doi:10.1038/s41590-018-0207-y
427 12. J. Cao, R. Dong, L. Jiang, Y. Gong, M. Yuan, J. You, W. Meng, Z. Chen, N.
428 Zhang, Q. Weng, H. Zhu, Q. He, M. Ying and B. Yang: LncRNA-MM2P Identified as
429 a Modulator of Macrophage M2 Polarization. *Cancer Immunology Research*, 7(2),
430 292-305 (2019) doi:10.1158/2326-6066.Cir-18-0145
431 13. M. I. Love, W. Huber and S. Anders: Moderated estimation of fold change and
432 dispersion for RNA-seq data with DESeq2. *Genome Biology*, 15(12), 550 (2014)
433 doi:10.1186/s13059-014-0550-8
434 14. J.-H. Li, S. Liu, H. Zhou, L.-H. Qu and J.-H. Yang: starBase v2.0: decoding
435 miRNA-ceRNA, miRNA-ncRNA and protein–RNA interaction networks from
436 large-scale CLIP-Seq data. *Nucleic Acids Research*, 42(D1), D92-D97 (2014)
437 doi:10.1093/nar/gkt1248
438 15. J.-H. Yang, J.-H. Li, P. Shao, H. Zhou, Y.-Q. Chen and L.-H. Qu: starBase: a
439 database for exploring microRNA–mRNA interaction maps from Argonaute
440 CLIP-Seq and Degradome-Seq data. *Nucleic Acids Research*, 39(suppl_1),
441 D202-D209 (2011) doi:10.1093/nar/gkq1056
442 16. P. Shannon, A. Markiel, O. Ozier, N. S. Baliga, J. T. Wang, D. Ramage, N. Amin,
443 B. Schwikowski and T. Ideker: Cytoscape: a software environment for integrated
444 models of biomolecular interaction networks. *Genome research*, 13(11), 2498-2504
445 (2003) doi:10.1101/gr.1239303
446 17. A. M. Newman, C. L. Liu, M. R. Green, A. J. Gentles, W. Feng, Y. Xu, C. D.
447 Hoang, M. Diehn and A. A. Alizadeh: Robust enumeration of cell subsets from tissue
448 expression profiles. *Nature methods*, 12(5), 453-457 (2015) doi:10.1038/nmeth.3337
449 18. X. Zhang, M. Wang, H. Sun, T. Zhu and X. Wang: Downregulation of
450 LINC00894-002 Contributes to Tamoxifen Resistance by Enhancing the TGF-β
451 Signaling Pathway. *Biochemistry (Moscow)*, 83(5), 603-611 (2018)
452 doi:10.1134/S0006297918050139

19. T. Liu, J. Sui, Y. Zhang, X. M. Zhang, W. J. Wu, S. Yang, S. Y. Xu, W. W. Hong, H. Peng, L. H. Yin, Y. P. Pu and G. Y. Liang: Comprehensive analysis of a novel lncRNA profile reveals potential prognostic biomarkers in clear cell renal cell carcinoma. *Oncol Rep*, 40(3), 1503-1514 (2018) doi:10.3892/or.2018.6540

20. A. Ward, A. Balwierz, J. D. Zhang, M. Küblbeck, Y. Pawitan, T. Hielscher, S. Wiemann and Ö. Sahin: Re-expression of microRNA-375 reverses both tamoxifen resistance and accompanying EMT-like properties in breast cancer. *Oncogene*, 32(9), 1173-1182 (2013) doi:10.1038/onc.2012.128

21. S.-M. Park, A. B. Gaur, E. Lengyel and M. E. Peter: The miR-200 family determines the epithelial phenotype of cancer cells by targeting the E-cadherin repressors ZEB1 and ZEB2. *Genes & development*, 22(7), 894-907 (2008) doi:10.1101/gad.1640608

22. M. Farhan, M. Aatif, P. Dandawate and A. Ahmad: Non-coding RNAs as Mediators of Tamoxifen Resistance in Breast Cancers. In: *Breast Cancer Metastasis and Drug Resistance: Challenges and Progress*. Ed A. Ahmad. Springer International Publishing, Cham (2019) doi:10.1007/978-3-030-20301-6_11

23. L. Huang, G. Liang, Q. Zhang and W. Zhao: The Role of Long Noncoding RNAs in Antiestrogen Resistance in Breast Cancer: An Overview and Update. *Journal of breast cancer*, 23(2), 129-140 (2020) doi:10.4048/jbc.2020.23.e10

24. X. Lai, S. K. Gupta, U. Schmitz, S. Marquardt, S. Knoll, A. Spitschak, O. Wolkenhauer, B. M. Pützer and J. Vera: MiR-205-5p and miR-342-3p cooperate in the repression of the E2F1 transcription factor in the context of anticancer chemotherapy resistance. *Theranostics*, 8(4), 1106-1120 (2018) doi:10.7150/thno.19904

25. Y. Qin, X. Zhou, C. Huang, L. Li, H. Liu, N. Liang, Y. Chen, D. Ma, Z. Han, X. Xu, J. He and S. Li: Serum miR-342-3p is a novel diagnostic and prognostic biomarker for non-small cell lung cancer. *International journal of clinical and experimental pathology*, 11(5), 2742-2748 (2018)

26. X. Xue, X. Fei, W. Hou, Y. Zhang, L. Liu and R. Hu: miR-342-3p suppresses cell proliferation and migration by targeting AGR2 in non-small cell lung cancer. *Cancer Letters*, 412, 170-178 (2018) doi:https://doi.org/10.1016/j.canlet.2017.10.024

27. X. Meng, J. Ma, B. Wang, X. Wu and Z. Liu: Long non-coding RNA OIP5-AS1 promotes pancreatic cancer cell growth through sponging miR-342-3p via AKT/ERK signaling pathway. *Journal of Physiology and Biochemistry*, 76(2), 301-315 (2020) doi:10.1007/s13105-020-00734-4

28. F. Zheng, H. Zhang and J. Lu: Identification of potential microRNAs and their targets in promoting gefitinib resistance by integrative network analysis. *Journal of thoracic disease*, 11(12), 5535-5546 (2019) doi:10.21037/jtd.2019.11.25

29. L. Deng, R. R. Broaddus, A. McCampbell, G. L. Shipley, D. S. Loose, G. M. Stancel, J. H. Pickar and P. J. A. Davies: Identification of a Novel Estrogen-Regulated Gene, EIG121, Induced by Hormone Replacement Therapy and Differentially Expressed in Type I and Type II Endometrial Cancer. *Clinical Cancer Research*, 11(23), 8258 (2005) doi:10.1158/1078-0432.CCR-05-1189

30. J. M. Kang, S. Park, S. J. Kim, H. Kim, B. Lee, J. Kim, J. Park, S. T. Kim, H.-K. Yang, W. H. Kim and S.-J. Kim: KIAA1324 Suppresses Gastric Cancer Progression by Inhibiting the Oncoprotein GRP78. *Cancer Research*, 75(15), 3087 (2015) doi:10.1158/0008-5472.CAN-14-3751

31. S. N. Westin, R. R. Broaddus, L. Deng, A. McCampbell, K. H. Lu, R. A. Lacour, M. R. Milam, D. L. Urbauer, P. Mueller, J. H. Pickar and D. S. Loose: Molecular clustering of endometrial carcinoma based on estrogen-induced gene expression. *Cancer biology & therapy*, 8(22), 2126-2135 (2009) doi:10.4161/cbt.8.22.9740

32. D. S. Oh, M. A. Troester, J. Usary, Z. Hu, X. He, C. Fan, J. Wu, L. A. Carey and C. M. Perou: Estrogen-Regulated Genes Predict Survival in Hormone Receptor–Positive Breast Cancers. *Journal of Clinical Oncology*, 24(11), 1656-1664 (2006) doi:10.1200/JCO.2005.03.2755

33. M. P. Schlumbrecht, S.-S. Xie, G. L. Shipley, D. L. Urbauer and R. R. Broaddus: Molecular clustering based on ERα and EIG121 predicts survival in high-grade serous carcinoma of the ovary/peritoneum. *Modern Pathology*, 24(3), 453-462 (2011) doi:10.1038/modpathol.2010.211

34. L. Deng, J. Feng and R. R. Broaddus: The novel estrogen-induced gene EIG121 regulates autophagy and promotes cell survival under stress. *Cell death & disease*, 1(4), e32-e32 (2010) doi:10.1038/cddis.2010.9

35. G. Zhu, L. Pei, H. Yin, F. Lin, X. Li, X. Zhu, W. He and X. Gou: Profiles of tumor-infiltrating immune cells in renal cell carcinoma and their clinical implications. *Oncology letters*, 18(5), 5235-5242 (2019) doi:10.3892/ol.2019.10896

36. S. Crotty: Follicular Helper CD4 T Cells (TFH). *Annual Review of Immunology*, 29(1), 621-663 (2011) doi:10.1146/annurev-immunol-031210-101400

37. S. Crotty: T Follicular Helper Cell Biology: A Decade of Discovery and Diseases. *Immunity*, 50(5), 1132-1148 (2019) doi:10.1016/j.immuni.2019.04.011

38. R. J. Johnston, A. C. Poholek, D. DiToro, I. Yusuf, D. Eto, B. Barnett, A. L. Dent, J. Craft and S. Crotty: Bcl6 and Blimp-1 are reciprocal and antagonistic regulators of T follicular helper cell differentiation. *Science (New York, N.Y.)*, 325(5943), 1006-1010 (2009) doi:10.1126/science.1175870

39. P. Amé-Thomas, J. Le Priol, H. Yssel, G. Caron, C. Pangault, R. Jean, N. Martin, T. Marafioti, P. Gaulard, T. Lamy, T. Fest, G. Semana and K. Tarte: Characterization of intratumoral follicular helper T cells in follicular lymphoma: role in the survival of malignant B cells. *Leukemia*, 26(5), 1053-1063 (2012) doi:10.1038/leu.2011.301

40. Z. Guo, H. Liang, Y. Xu, L. Liu, X. Ren, S. Zhang, S. Wei and P. Xu: The Role of Circulating T Follicular Helper Cells and Regulatory Cells in Non-Small Cell Lung Cancer Patients. *Scandinavian Journal of Immunology*, 86(2), 107-112 (2017) doi:https://doi.org/10.1111/sji.12566

41. C. Gu-Trantien, S. Loi, S. Garaud, C. Equeter, M. Libin, A. de Wind, M. Ravoet, H. Le Buanec, C. Sibille, G. Manfouo-Foutsop, I. Veys, B. Haibe-Kains, S. K. Singhal, S. Michiels, F. Rothé, R. Salgado, H. Duvillier, M. Ignatiadis, C. Desmedt, D. Bron, D. Larsimont, M. Piccart, C. Sotiriou and K. Willard-Gallo: CD4 follicular helper T

cell infiltration predicts breast cancer survival. *The Journal of clinical investigation*, 123(7), 2873-2892 (2013) doi:10.1172/JCI67428

42. G. Bindea, B. Mlecnik, M. Tosolini, A. Kirilovsky, M. Waldner, Anna C. Obenauf, H. Angell, T. Fredriksen, L. Lafontaine, A. Berger, P. Bruneval, Wolf H. Fridman, C. Becker, F. Pagès, Michael R. Speicher, Z. Trajanoski and J. Galon: Spatiotemporal Dynamics of Intratumoral Immune Cells Reveal the Immune Landscape in Human Cancer. *Immunity*, 39(4), 782-795 (2013) doi:https://doi.org/10.1016/j.immuni.2013.10.003

43. B. Frossi, F. Mion, C. Tripodo, M. P. Colombo and C. E. Pucillo: Rheostatic Functions of Mast Cells in the Control of Innate and Adaptive Immune Responses. *Trends in Immunology*, 38(9), 648-656 (2017) doi:https://doi.org/10.1016/j.it.2017.04.001

44. E. Z. M. da Silva, M. C. Jamur and C. Oliver: Mast cell function: a new vision of an old cell. *The journal of histochemistry and cytochemistry : official journal of the Histochemistry Society*, 62(10), 698-738 (2014) doi:10.1369/0022155414545334

45. C. Wang, X. Tang, J. Wang and Y. Xu: Patterns of immune infiltration in lung adenocarcinoma revealed a prognosis-associated microRNA–mast cells network. *Human Cell*, 33(1), 205-219 (2020) doi:10.1007/s13577-019-00300-1

46. N. Rohr-Udilova, F. Klinglmüller, R. Schulte-Hermann, J. Stift, M. Herac, M. Salzmann, F. Finotello, G. Timelthaler, G. Oberhuber, M. Pinter, T. Reiberger, E. Jensen-Jarolim, R. Eferl and M. Trauner: Deviations of the immune cell landscape between healthy liver and hepatocellular carcinoma. *Scientific reports*, 8(1), 6220-6220 (2018) doi:10.1038/s41598-018-24437-5

Figure Captions

Figure 1 Flowchart of the analysis process.

Figure 2 Genes differentially expressed in 506 KIRC tissues versus 71 normal adjacent tissues. Provided are the heatmap (a) and the volcano plot (b) of 357 differentially expressed lncRNAs between the two groups; the heatmap (c) and the volcano plot (d) of 132 differentially expressed miRNAs between the two groups; and the heatmap (e) and the volcano plot (f) of 3092 differentially expressed protein-coding genes between the two groups; and the composition of differentially expressed genes (g). All differentially expressed genes had a log (fold-change) > 1.0 or < -1.0 and the overall of FDR < 0.05.

Figure 3 (a) The KIRC related ceRNA network consisting of 12 lncRNAs, 25 miRNAs and 136 mRNAs. (b-j) The K-M survival curves of the top three lncRNAs, miRNAs and mRNAs: PVT1 (b), AC005154.1 (c), AC015813.1 (d), hsa-miR-21-5p (e), hsa-miR-130b-3p (f), hsa-miR-204-5p (g), MXD3 (h), VPS13D (i) and KCNN4 (j).

Figure 4 The Cox proportional hazards regression model (a) based on RNAs screened

by Lasso regression analysis (b and c) in the ceRNA network. Seven potential prognosis related RNAs were integrated into the Cox proportional hazards regression model. The nomogram (e) was constructed based on the model. The ROC (d) and calibration curves (f) indicate the acceptable accuracy (AUCs of 1, 3 and 5-year survivals: 0.779, 0.747 and 0.772) and discrimination of the nomogram.

*$P < 0.05$; **$P < 0.010$; ***$P < 0.001$.

Figure 5 The composition (a) and heatmap (b) of immune cells estimated by the CIBERSORT algorithm in five normal adjacent tissues and 206 KIRC tissues. The violin plot of immune cells (c) compares cells' proportion between the two groups.

Figure 6 The Cox proportional hazards regression model (a) based on immune cells screened by Lasso regression analysis (b and c). Tfh cells and resting mast cells were integrated into the Cox proportional hazards regression model. The nomogram (e) was constructed based on the model. The ROC (d) and the calibration curves (f) indicate the acceptable accuracy (AUCs of 1, 3 and 5-year survivals: 0.603, 0.642 and 0.607) and discrimination of the nomogram.

*$P < 0.05$; **$P < 0.010$; ***$P < 0.001$.

Figure 7 Co-expression heatmap of all immune cells in KIRC (a); the co-expression heatmap of the RNAs and immune cells in the two Cox proportional hazards regression models (b); the significant results of Pearson correlation coefficients between the RNAs and immune cells: Tfh cells and LINC00894 (c); Tfh cells and KIAA1324 (d); resting mast cells and LINC00894 (e); resting mast cells and KIAA1324 (f).

619 **Table**

620

Table 1 Hypergeometric testing and correlation analysis results of ceRNAs pairs

lncRNAs	mRNAs	miRNAs	Hypergeometric test *P*	Correlation *P*
AC005154.1	KAT2A	hsa-miR-122-5p	0.042851557	1.32E-95
AC015813.1	SLC16A1	hsa-miR-590-3p	0.0433213	0.019445968
AC015813.1	FHOD1	hsa-miR-590-3p	0.007220217	4.09E-19
AC015813.1	E2F8	hsa-miR-590-3p	0.025270758	1.22E-09
AC015813.1	SERPINB9	hsa-miR-590-3p	0.025270758	0.000636067
AC015813.1	COL5A2	hsa-miR-590-3p	0.014440433	0.015398545
AC015813.1	BRIP1	hsa-miR-590-3p	0.003610108	5.18E-09
AC015813.1	ESCO2	hsa-miR-590-3p	0.02166065	0.009163956
AC015813.1	TXLNB	hsa-miR-590-3p	0.003610108	0.020621823

AC015813.1	PSTPIP2	hsa-miR-590-3p	0.003610108	0.000108913
AC015813.1	SNRNP70	hsa-miR-590-3p	0.003610108	4.80E-73
AC016876.2	TNFRSF10B	hsa-miR-133a-3p	0.003810813	9.33E-39
AC016876.2	MYO9B	hsa-miR-133a-3p	0.000392403	1.06E-53
AC016876.2	PREX1	hsa-miR-133a-3p	0.013191013	2.17E-22
AC016876.2	CAPN15	hsa-miR-133a-3p	0.027474351	1.51E-34
AC016876.2	CORO1C	hsa-miR-133a-3p	0.001461641	2.06E-36
AC016876.2	FJX1	hsa-miR-133a-3p	0.036258784	6.66E-19
AC016876.2	NDRG1	hsa-miR-133a-3p	0.010361047	1.00E-11
AC016876.2	VKORC1	hsa-miR-133a-3p	0.001165794	1.01E-27
AC016876.2	TMEM200B	hsa-miR-133a-3p	0.013191013	9.12E-19
AC016876.2	RSRP1	hsa-miR-133a-3p	0.000881161	6.23E-07

C1RL-AS1	SCARB1	hsa-miR-16-5p	0.001438811	1.64E-42
C1RL-AS1	VEGFA	hsa-miR-16-5p	0.030764401	2.81E-61
C1RL-AS1	AHNAK2	hsa-miR-16-5p	0.000392403	7.17E-21
C1RL-AS1	PTHLH	hsa-miR-16-5p	0.009888558	1.10E-07
C1RL-AS1	RELT	hsa-miR-16-5p	0.000732486	3.61E-14
C1RL-AS1	PFKFB4	hsa-miR-16-5p	0.004002511	6.80E-27
C1RL-AS1	CCND1	hsa-miR-16-5p	0.046303563	7.81E-25
C1RL-AS1	APLN	hsa-miR-16-5p	0.000549364	2.74E-25
C1RL-AS1	SH2D2A	hsa-miR-16-5p	0.000732486	7.13E-19
C1RL-AS1	SEL1L3	hsa-miR-16-5p	0.012975462	1.23E-23
C1RL-AS1	UNC5B	hsa-miR-16-5p	0.000392403	1.58E-15
C1RL-AS1	PHLDA3	hsa-miR-16-5p	0.001177209	0.000714118

C1RL-AS1	SLC41A2	hsa-miR-16-5p	0.000941767	1.16E-10
C1RL-AS1	GRB10	hsa-miR-16-5p	0.022523937	4.08E-21
C1RL-AS1	SLC2A3	hsa-miR-16-5p	0.013812588	1.39E-09
C1RL-AS1	MYBL1	hsa-miR-16-5p	0.049468948	1.21E-08
C1RL-AS1	ANLN	hsa-miR-16-5p	0.004002511	7.40E-05
C1RL-AS1	OTOGL	hsa-miR-16-5p	0.000392403	1.38E-08
C1RL-AS1	KCNJ2	hsa-miR-16-5p	0.019384712	9.72E-07
C1RL-AS1	CNTNAP1	hsa-miR-16-5p	0.003139225	6.23E-12
C1RL-AS1	NRARP	hsa-miR-16-5p	0.023622665	4.17E-13
C1RL-AS1	CREB5	hsa-miR-16-5p	0.013812588	5.44E-48
C1RL-AS1	ATAD5	hsa-miR-16-5p	0.042928897	2.56E-37
C1RL-AS1	INSR	hsa-miR-16-5p	0.009182232	1.03E-20

C1RL-AS1	SIPA1L2	hsa-miR-16-5p	0.006043007	9.08E-08
C1RL-AS1	AATK	hsa-miR-16-5p	0.000549364	1.52E-28
C1RL-AS1	RFLNB	hsa-miR-16-5p	0.000941767	5.34E-05
C1RL-AS1	SPRY4	hsa-miR-16-5p	0.002746822	8.52E-14
C1RL-AS1	ARL10	hsa-miR-16-5p	0.001438811	1.17E-11
C1RL-AS1	ANKRD13B	hsa-miR-16-5p	0.003139225	7.32E-16
C1RL-AS1	SNAP25	hsa-miR-16-5p	0.002380579	1.30E-19
C1RL-AS1	LY6E	hsa-miR-16-5p	0.000941767	1.68E-17
C1RL-AS1	CDK5R1	hsa-miR-16-5p	0.013812588	1.69E-16
C1RL-AS1	CLCN5	hsa-miR-16-5p	0.006618532	0.020236846
C1RL-AS1	BDNF	hsa-miR-16-5p	0.010621043	8.30E-09
C1RL-AS1	IRX3	hsa-miR-16-5p	0.000732486	1.79E-37

C1RL-AS1	PLAGL1	hsa-miR-16-5p	0.004473395	1.30E-23
C1RL-AS1	IRF4	hsa-miR-16-5p	0.004970439	2.67E-12
C1RL-AS1	TSPYL2	hsa-miR-16-5p	0.002380579	1.01E-20
C1RL-AS1	TLL1	hsa-miR-16-5p	0.007848062	5.19E-19
C1RL-AS1	KCNN4	hsa-miR-16-5p	0.000732486	4.96E-09
C1RL-AS1	TRIM36	hsa-miR-16-5p	0.015565322	0.000352309
C1RL-AS1	CBFA2T3	hsa-miR-16-5p	0.004970439	6.86E-13
C1RL-AS1	TSC22D3	hsa-miR-16-5p	0.012975462	3.07E-05
C1RL-AS1	SNCG	hsa-miR-16-5p	0.001726574	0.02336615
EPB41L4A-AS1	TNFRSF10B	hsa-miR-93-5p	0.005296055	0.000309792
EPB41L4A-AS1	IKBIP	hsa-miR-93-5p	0.049992152	1.07E-06
H19	EGLN3	hsa-miR-130b-3p	0.025364366	0.030923622

H19	UXS1	hsa-miR-130b-3p	0.017341521	0.000663666
H19	USP46	hsa-miR-130b-3p	0.024521918	0.043104031
H19	ACSL4	hsa-miR-130b-3p	0.049356887	0.046472711
H19	LDLRAD3	hsa-miR-130b-3p	0.017341521	2.91E-06
H19	BMP6	hsa-miR-130b-3p	0.021136246	1.44E-05
H19	RASD1	hsa-miR-130b-3p	0.001092495	0.000237995
H19	NHSL1	hsa-miR-130b-3p	0.002162624	0.000635296
H19	C8orf4	hsa-miR-130b-3p	0.040677495	1.83E-10
H19	MAP3K12	hsa-miR-130b-3p	0.000287237	0.006322847
H19	VPS13D	hsa-miR-130b-3p	0.00310273	0.022110203
H19	PXDN	hsa-miR-130b-3p	0.001415171	2.64E-12
H19	PMEPA1	hsa-miR-130b-3p	0.001092495	2.21E-10

H19	WNK3	hsa-miR-130b-3p	0.000207327	0.000409846
H19	PFKFB3	hsa-miR-130b-3p	0.004199543	0.001757017
H19	TCF4	hsa-miR-130b-3p	0.000309855	2.83E-07
H19	HECW2	hsa-miR-130b-3p	0.001092495	0.000515485
H19	LRRC41	hsa-miR-130b-3p	0.008478302	0.004641957
H19	KLHL3	hsa-miR-130b-3p	0.035134428	0.004796761
H19	LDLR	hsa-miR-130b-3p	0.002491825	6.36E-13
H19	SCARA3	hsa-miR-130b-3p	0.005054152	6.50E-06
LINC00893	SCARB1	hsa-miR-125b-5p, hsa-miR-125a-5p	0.001438811	0.000105621
LINC00893	VEGFA	hsa-miR-125b-5p, hsa-miR-125a-5p	0.030764401	8.10E-26
LINC00893	MYEOV	hsa-miR-125b-5p	0.014414273	6.39E-05
LINC00893	SOX11	hsa-miR-125b-5p, hsa-miR-125a-5p	0.015565322	9.42E-07

LINC00893	PRDM1	hsa-miR-125b-5p, hsa-miR-125a-5p	0.032046251	0.001791829
LINC00893	GJC1	hsa-miR-125b-5p, hsa-miR-125a-5p	0.003139225	1.58E-05
LINC00893	OLFML2A	hsa-miR-125b-5p, hsa-miR-125a-5p	0.000156961	0.009879398
LINC00893	LIMD2	hsa-miR-125b-5p, hsa-miR-125a-5p	0.006043007	8.66E-13
LINC00893	GRB10	hsa-miR-125b-5p, hsa-miR-125a-5p	0.022523937	0.004617551
LINC00893	TNFAIP3	hsa-miR-125b-5p, hsa-miR-125a-5p	0.02040496	0.000292635
LINC00893	KMT5C	hsa-miR-125b-5p, hsa-miR-125a-5p	0.006618532	1.47E-81
LINC00893	PDE7A	hsa-miR-125b-5p, hsa-miR-125a-5p	0.019384712	2.94E-13
LINC00893	PLAGL1	hsa-miR-125b-5p, hsa-miR-125a-5p	0.004473395	1.50E-09
LINC00893	IRF4	hsa-miR-125b-5p, hsa-miR-125a-5p	0.004970439	8.51E-05
LINC00893	FAM118A	hsa-miR-125b-5p, hsa-miR-125a-5p	0.005493643	1.23E-43
LINC00894	GRIN2D	hsa-miR-342-3p	0.02166065	0.020258812

MALAT1	ZNF395	hsa-miR-429, hsa-miR-200c-3p	0.033565927	0.009006143
MALAT1	SCD	hsa-miR-200b-3p, hsa-miR-200a-3p, hsa-miR-429, hsa-miR-200c-3p, hsa-miR-141-3p	0.039289444	0.011807116
MALAT1	EZH2	hsa-miR-217	0.039289444	6.86E-14
MALAT1	MXD3	hsa-miR-200b-3p, hsa-miR-429, hsa-miR-200c-3p	0.001707738	3.90E-34
MALAT1	BAZ1A	hsa-miR-590-3p	0.018390826	7.26E-05
MALAT1	SIX1	hsa-miR-200b-3p, hsa-miR-200a-3p, hsa-miR-429, hsa-miR-200c-3p, hsa-miR-141-3p, hsa-miR-590-3p	0.00025153	4.87E-06
MALAT1	KCNJ2	hsa-miR-1-3p, hsa-miR-1271-5p, hsa-miR-590-3p	0.000680978	0.01227854
MALAT1	RUNX2	hsa-miR-203a-3p, hsa-miR-217, hsa-miR-590-3p	0.027070651	0.007921587
MALAT1	PDE7A	hsa-miR-1-3p	0.031465278	1.64E-07
MALAT1	CCND2	hsa-miR-200a-3p, hsa-miR-141-3p, hsa-miR-1-3p,	0.002367103	0.005749454

		hsa-miR-1271-5p		
MALAT1	FOXF1	hsa-miR-200b-3p, hsa-miR-429, hsa-miR-200c-3p	0.033565927	0.001701238
MALAT1	KIAA1324	hsa-miR-1271-5p	0.040612149	0.018453328
NEAT1	STC2	hsa-miR-181b-5p, hsa-miR-204-5p	0.005508592	0.022782701
NEAT1	GJC1	hsa-let-7e-5p, hsa-let-7g-5p	0.010508709	0.038550157
NEAT1	ADM	hsa-miR-181b-5p	0.028501136	9.33E-08
NEAT1	EZH2	hsa-let-7e-5p, hsa-let-7g-5p	0.008654278	1.27E-12
NEAT1	AURKB	hsa-let-7e-5p, hsa-let-7g-5p	0.00048449	0.032101352
NEAT1	KIF21B	hsa-let-7e-5p, hsa-let-7g-5p	0.003786827	3.94E-06
NEAT1	INTS6L	hsa-let-7e-5p, hsa-let-7g-5p	0.001348287	1.00E-46
NEAT1	DTX2	hsa-let-7e-5p, hsa-let-7g-5p	0.022864398	0.003873252
NEAT1	LIMD2	hsa-let-7e-5p, hsa-let-7g-5p	0.001852057	0.023584192

NEAT1	NGF	hsa-let-7e-5p, hsa-let-7g-5p	0.00048449	0.036481826
NEAT1	POLQ	hsa-miR-181b-5p, hsa-let-7e-5p	0.026346413	4.13E-05
NEAT1	POU2F2	hsa-let-7e-5p, hsa-let-7g-5p	0.00772659	0.046579228
NEAT1	APBB3	hsa-let-7e-5p, hsa-let-7g-5p	0.003786827	1.03E-93
NEAT1	MAPK11	hsa-let-7e-5p, hsa-let-7g-5p	0.00048449	0.020903367
NEAT1	FBXO41	hsa-miR-181b-5p	0.000291346	0.00718285
NEAT1	PITPNM3	hsa-let-7e-5p, hsa-let-7g-5p	0.022864398	0.000826877
NEAT1	NPHP3	hsa-let-7e-5p, hsa-let-7g-5p	0.022864398	7.31E-68
NEAT1	DNA2	hsa-let-7e-5p, hsa-let-7g-5p	0.003786827	1.69E-34
NEAT1	AMT	hsa-let-7e-5p, hsa-let-7g-5p	0.000906364	0.001503922
NEAT1	SLC25A37	hsa-miR-181b-5p	0.002491825	1.48E-28
NEAT1	FAM118A	hsa-let-7e-5p, hsa-let-7g-5p	0.034971322	7.22E-34

NEAT1	AASS	hsa-let-7e-5p, hsa-let-7g-5p	0.00048449	1.39E-05
NEAT1	CELSR3	hsa-miR-181b-5p, hsa-miR-204-5p	0.00026878	5.77E-21
NEAT1	KIFC2	hsa-let-7e-5p, hsa-let-7g-5p	0.002491825	4.59E-65
NEAT1	RNF165	hsa-let-7e-5p, hsa-let-7g-5p	0.00587435	2.76E-05
NEAT1	SLC25A27	hsa-let-7e-5p, hsa-let-7g-5p	0.001554187	2.36E-89
PVT1	TNFRSF10B	hsa-miR-93-5p	0.005296055	1.15E-70
PVT1	IKBIP	hsa-miR-93-5p	0.049992152	4.69E-68
PVT1	TET3	hsa-miR-93-5p, hsa-miR-20b-5p	0.000351901	6.58E-37
PVT1	CCND2	hsa-miR-93-5p, hsa-miR-20b-5p	0.000180512	2.67E-22
SNHG1	NETO2	hsa-miR-21-5p	0.041029046	3.64E-18
SNHG1	CDKN2C	hsa-miR-154-5p	0.02166065	9.52E-06
SNHG1	GBP1	hsa-miR-21-5p	0.02166065	0.014315805

SNHG1	ADGRG2	hsa-miR-21-5p	0.00064624	1.35E-05

621

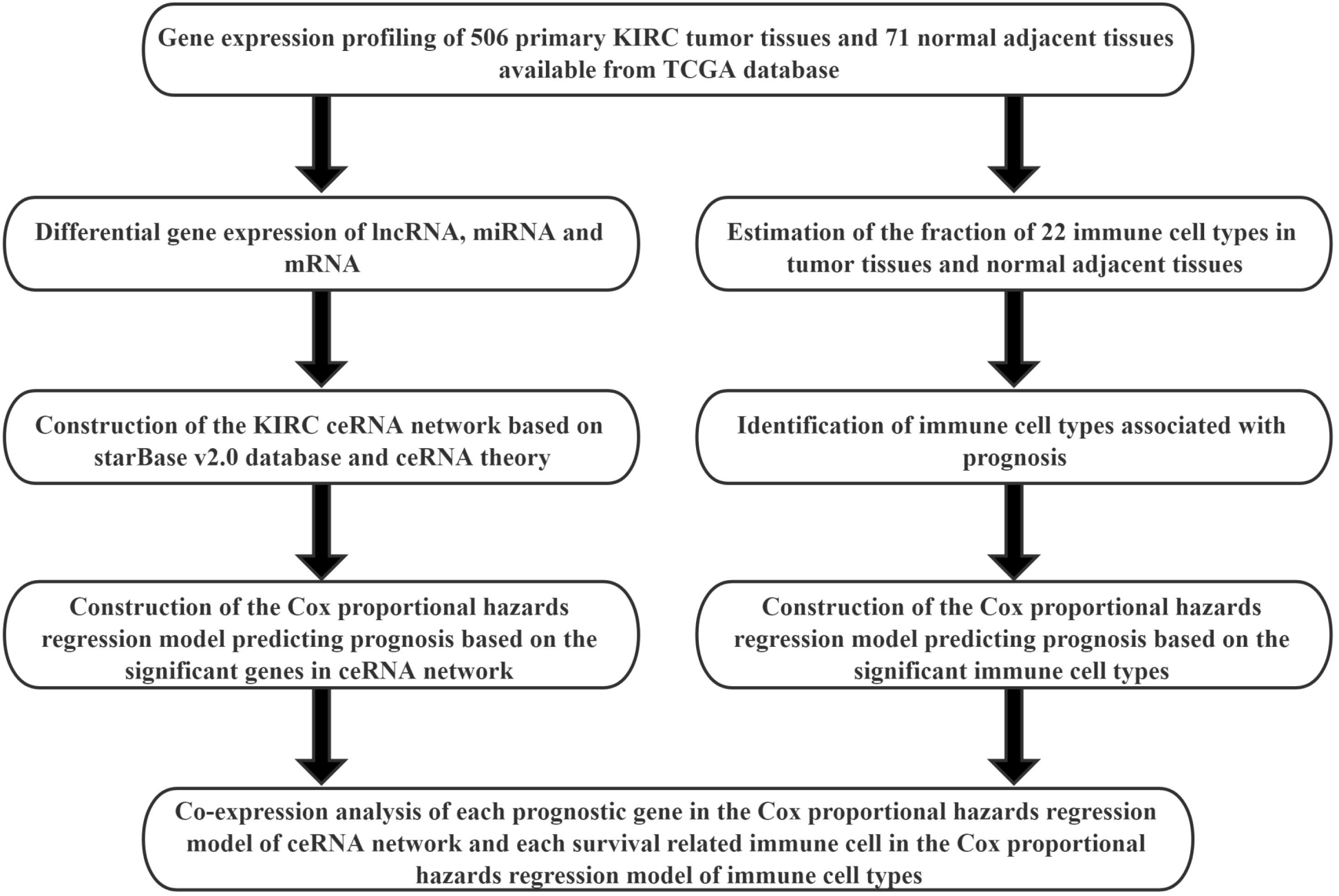
Gene expression profiling of 506 primary KIRC tumor tissues and 71 normal adjacent tissues available from TCGA database
Differential gene expression of lncRNA, miRNA and mRNA
Estimation of the fraction of 22 immune cell types in tumor tissues and normal adjacent tissues
Construction of the KIRC ceRNA network based on starBase v2.0 database and ceRNA theory
Identification of immune cell types associated with prognosis
Construction of the Cox proportional hazards regression model predicting prognosis based on the significant genes in ceRNA network
Construction of the Cox proportional hazards regression model predicting prognosis based on the significant immune cell types
Co-expression analysis of each prognostic gene in the Cox proportional hazards regression model of ceRNA network and each survival related immune cell in the Cox proportional hazards regression model of immune cell types

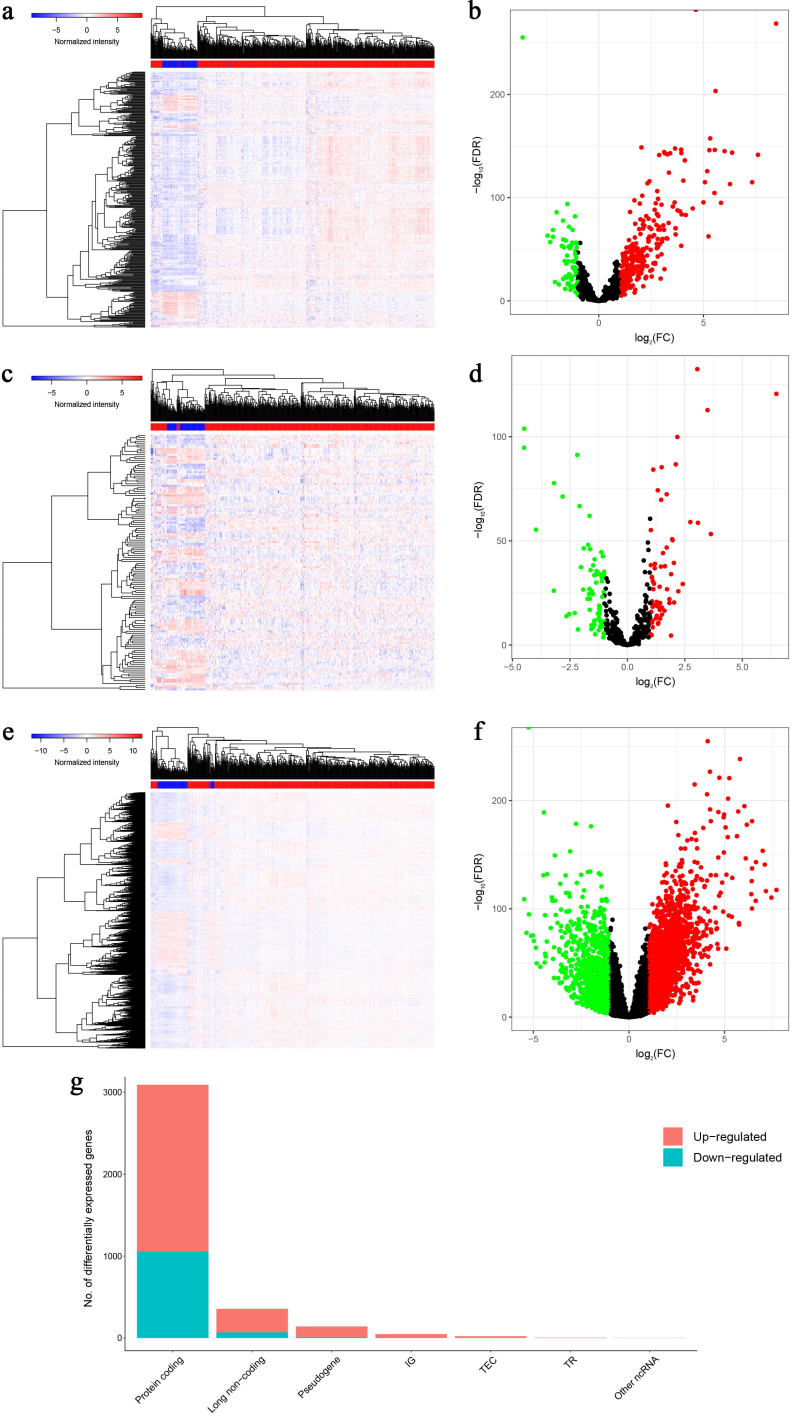
a
Normalized intensity
b
−log10(FDR)
log2(FC)
c
Normalized intensity
d
−log10(FDR)
log2(FC)
e
Normalized intensity
f
−log10(FDR)
log2(FC)
g
No. of differentially expressed genes
Up−regulated
Down−regulated
Protein coding
Long non−coding
Pseudogene
IG
TEC
TR
Other ncRNA

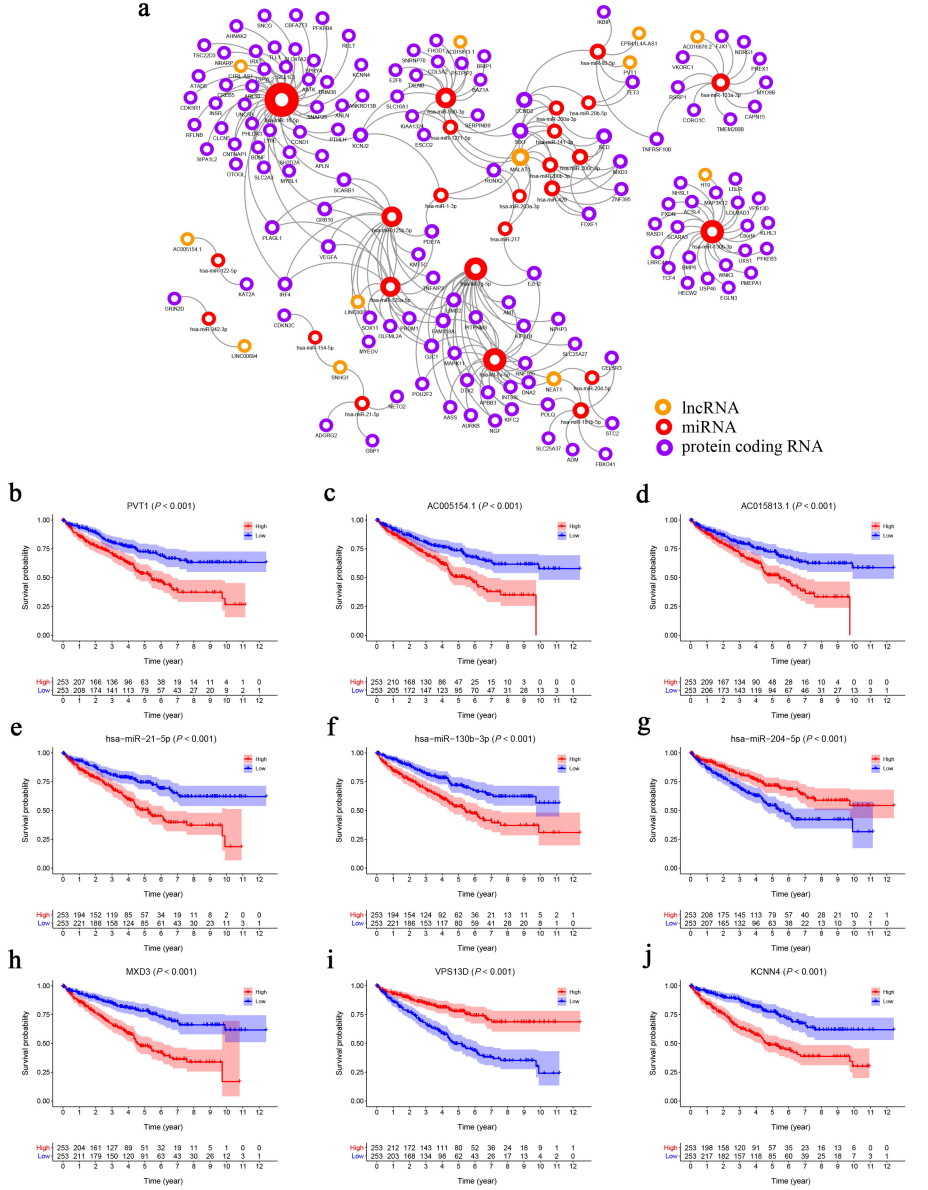
a
lncRNA
miRNA
protein coding RNA
b
PVT1 (P < 0.001)
c
AC005154.1 (P < 0.001)
d
AC015813.1 (P < 0.001)
e
hsa−miR−21−5p (P < 0.001)
f
hsa−miR−130b−3p (P < 0.001)
g
hsa−miR−204−5p (P < 0.001)
h
MXD3 (P < 0.001)
i
VPS13D (P < 0.001)
j
KCNN4 (P < 0.001)
Survival probability
Time (year)
High
Low

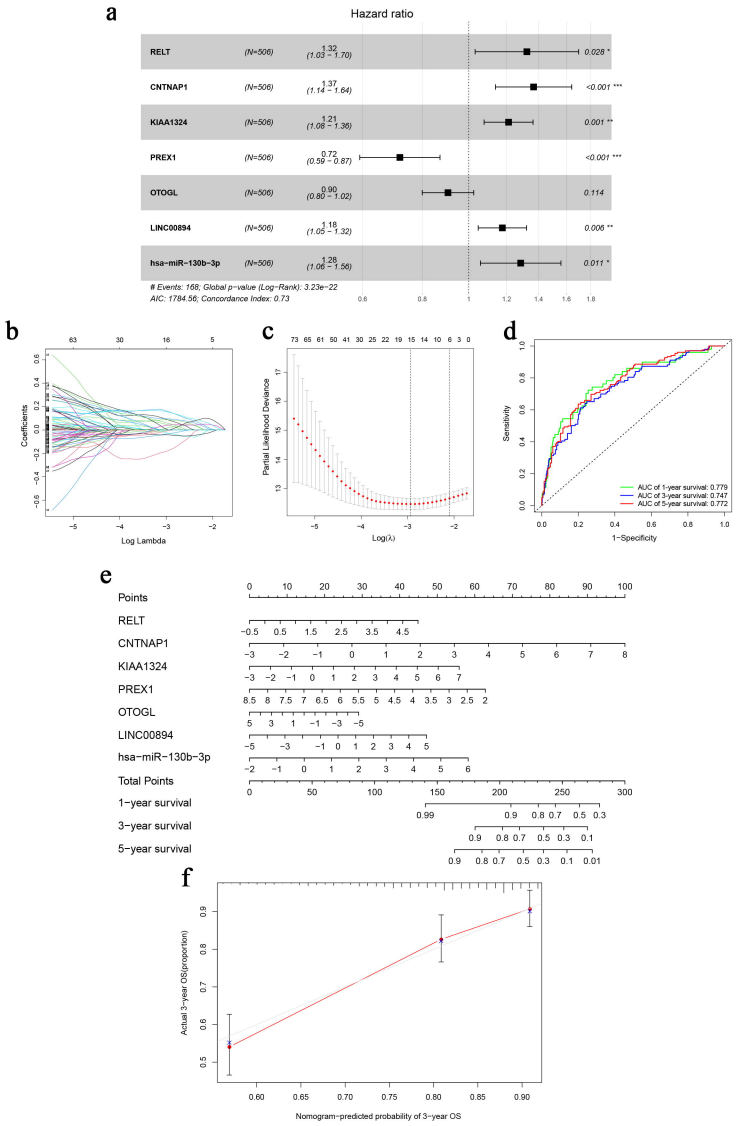
a
Hazard ratio
RELT (N=506) 1.32 (1.03 − 1.70) 0.028 *
CNTNAP1 (N=506) 1.37 (1.14 − 1.64) <0.001 ***
KIAA1324 (N=506) 1.21 (1.08 − 1.36) 0.001 **
PREX1 (N=506) 0.72 (0.59 − 0.87) <0.001 ***
OTOGL (N=506) 0.90 (0.80 − 1.02) 0.114
LINC00894 (N=506) 1.18 (1.05 − 1.32) 0.006 **
hsa−miR−130b−3p (N=506) 1.28 (1.06 − 1.56) 0.011 *
Events: 168; Global p−value (Log−Rank): 3.23e−22
AIC: 1784.56; Concordance Index: 0.73
0.6 0.8 1 1.2 1.4 1.6 1.8
b
Coefficients
Log Lambda
c
Partial Likelihood Deviance
Log(λ)
d
Sensitivity
1−Specificity
AUC of 1-year survival: 0.779
AUC of 3-year survival: 0.747
AUC of 5-year survival: 0.772
e
Points
RELT
CNTNAP1
KIAA1324
PREX1
OTOGL
LINC00894
hsa−miR−130b−3p
Total Points
1−year survival
3−year survival
5−year survival
f
Actual 3−year OS(proportion)
Nomogram−predicted probability of 3−year OS

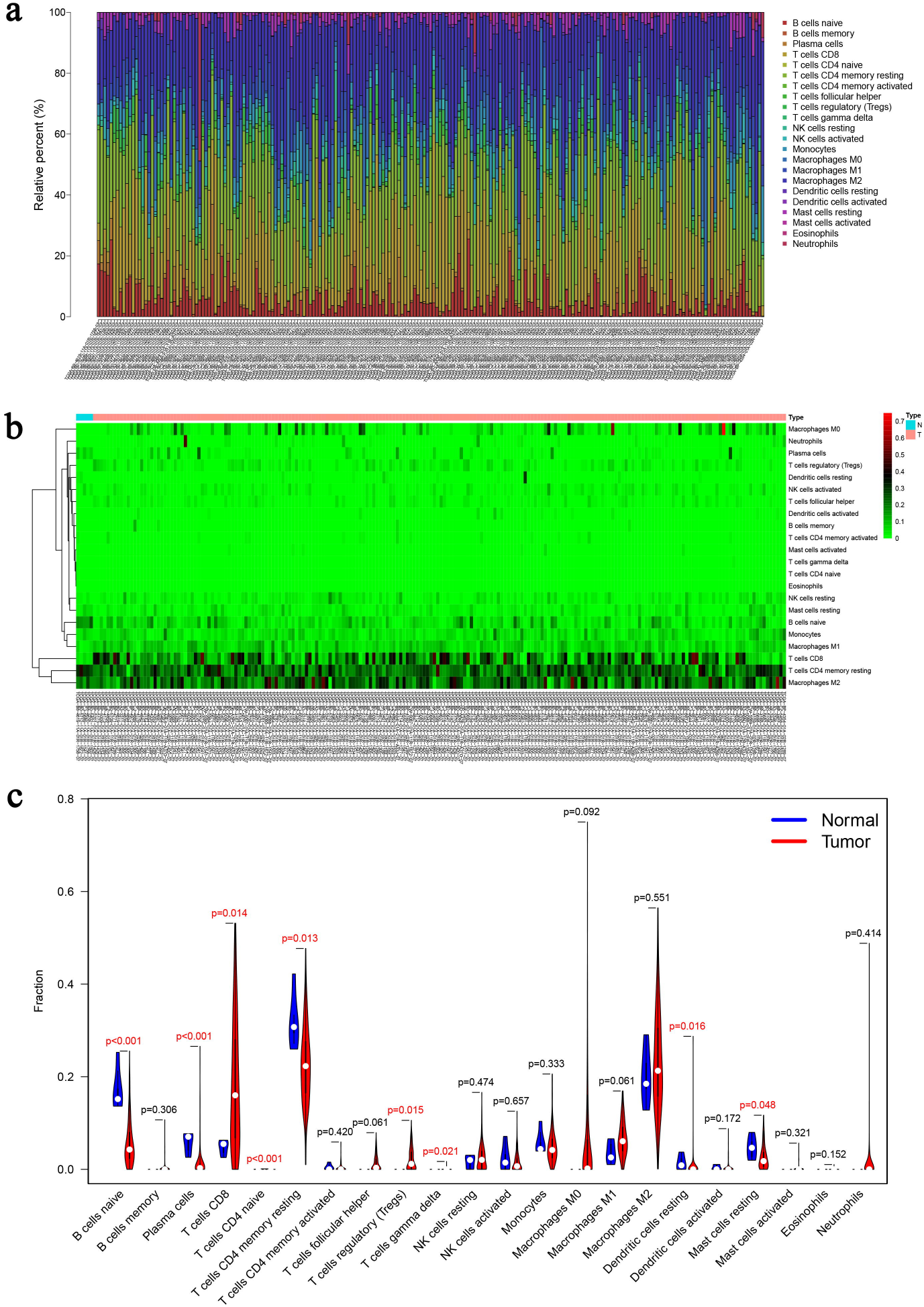
a
Relative percent (%)
100
80
60
40
20
0
B cells naive
B cells memory
Plasma cells
T cells CD8
T cells CD4 naive
T cells CD4 memory resting
T cells CD4 memory activated
T cells follicular helper
T cells regulatory (Tregs)
T cells gamma delta
NK cells resting
NK cells activated
Monocytes
Macrophages M0
Macrophages M1
Macrophages M2
Dendritic cells resting
Dendritic cells activated
Mast cells resting
Mast cells activated
Eosinophils
Neutrophils
b
Type
Macrophages M0
Neutrophils
Plasma cells
T cells regulatory (Tregs)
Dendritic cells resting
NK cells activated
T cells follicular helper
Dendritic cells activated
B cells memory
T cells CD4 memory activated
Mast cells activated
T cells gamma delta
T cells CD4 naive
Eosinophils
NK cells resting
Mast cells resting
B cells naive
Monocytes
Macrophages M1
T cells CD8
T cells CD4 memory resting
Macrophages M2
Type
N
T
0.7
0.6
0.5
0.4
0.3
0.2
0.1
0
c
Fraction
0.8
0.6
0.4
0.2
0.0
Normal
Tumor
p<0.001
p=0.306
p<0.001
p=0.014
p<0.001
p=0.013
p=0.420
p=0.061
p=0.015
p=0.021
p=0.474
p=0.657
p=0.333
p=0.092
p=0.061
p=0.551
p=0.016
p=0.172
p=0.048
p=0.321
p=0.152
p=0.414
B cells naive
B cells memory
Plasma cells
T cells CD8
T cells CD4 naive
T cells CD4 memory resting
T cells CD4 memory activated
T cells follicular helper
T cells regulatory (Tregs)
T cells gamma delta
NK cells resting
NK cells activated
Monocytes
Macrophages M0
Macrophages M1
Macrophages M2
Dendritic cells resting
Dendritic cells activated
Mast cells resting
Mast cells activated
Eosinophils
Neutrophils

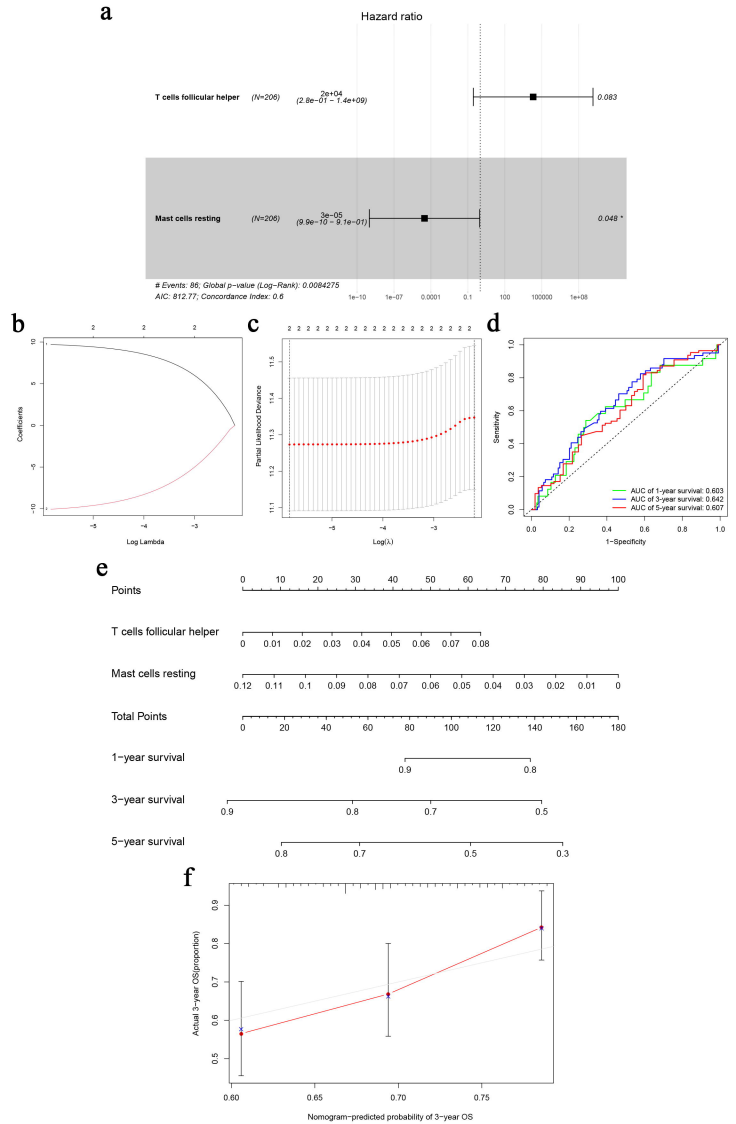
a
Hazard ratio
T cells follicular helper (N=206) 2e+04 (2.8e−01 − 1.4e+09) 0.083
Mast cells resting (N=206) 3e−05 (9.9e−10 − 9.1e−01) 0.048 *
Events: 86; Global p−value (Log−Rank): 0.0084275
AIC: 812.77; Concordance Index: 0.6
1e−10 1e−07 0.0001 0.1 100 100000 1e+08
b
Coefficients
Log Lambda
c
Partial Likelihood Deviance
Log(λ)
d
Sensitivity
1−Specificity
AUC of 1-year survival: 0.603
AUC of 3-year survival: 0.642
AUC of 5-year survival: 0.607
e
Points
T cells follicular helper
Mast cells resting
Total Points
1−year survival
3−year survival
5−year survival
f
Actual 3−year OS(proportion)
Nomogram−predicted probability of 3−year OS

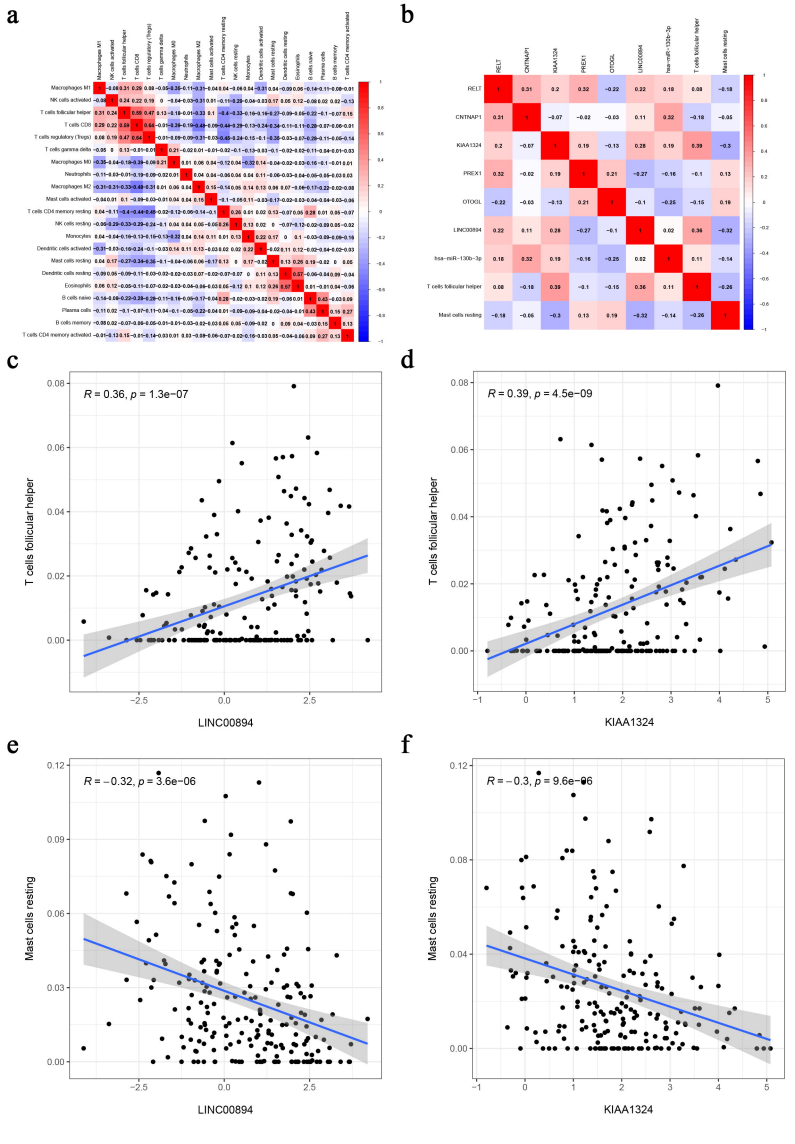
a
b
c
d
e
f
R = 0.36, p = 1.3e−07
T cells follicular helper
LINC00894
R = 0.39, p = 4.5e−09
T cells follicular helper
KIAA1324
R = −0.32, p = 3.6e−06
Mast cells resting
LINC00894
R = −0.3, p = 9.6e−06
Mast cells resting
KIAA1324